Hedayat, H., Sayers, C. J., Bugini, D., Dallera, C., Wolverson, D., Batten, T., ... Como, E. D. (2019). Excitonic and lattice contributions to the charge density wave in 1T-TiSe2 revealed by a phonon bottleneck. Manuscript submitted for publication.

Early version, also known as pre-print

Excitonic and lattice contributions to the charge density wave in 1*T*-$TiSe_2$ revealed by a phonon bottleneck.

H. Hedayat[1], C. J. Sayers[2], D. Bugini[1], C. Dallera[1], D. Wolverson[2], T. Batten[3], S. Karbassi[4], S. Friedemann[4], G. Cerullo[1], J. van Wezel[5], S.R. Clark[4,6], E. Carpene[7], E. Da Como[2]

1 Dipartimento di Fisica, Politecnico di Milano, 20133 Milano, Italy

2 Department of Physics, Centre Nanoscience and Nanotechnology (CNAN) and Centre for Photonics and Photonic Materials (CPPM), University of Bath, BA2 7AY Bath, UK

3 Renishaw plc., Wotton-under-Edge, GL12 7DW, UK

4 HH Wills Physics Laboratory, University of Bristol, BS8 1TL Bristol UK

5 Institute for Theoretical Physics, Institute of Physics, University of Amsterdam, 1090 GL Amsterdam, The Netherlands

6 Max Planck Institute for the Structure and Dynamics of Matter, CFEL, Hamburg, Germany

7 IFN-CNR, Dipartimento di Fisica, Politecnico di Milano, 20133 Milano, Italy

Abstract

Understanding collective electronic states such as superconductivity and charge density waves is pivotal for fundamental science and applications. The layered transition metal dichalcogenide 1*T*-$TiSe_2$ hosts a unique charge density wave (CDW) phase transition whose origins are still not fully understood. Here, we present ultrafast time- and angle-resolved photoemission spectroscopy (TR-ARPES) measurements complemented by time-resolved reflectivity (TRR) which allows us to establish the contribution of excitonic and electron-phonon interactions to the CDW. We monitor the energy shift of the valence band (VB) and coupling to coherent phonons as a function of laser fluence. The VB shift, directly related to the CDW gap closure, exhibits a markedly slower recovery dynamics at fluences above F_{th} = 60 μJ cm^{-2}. This observation coincides with a shift in the relative weight of coherently coupled phonons to higher frequency modes in time-resolved reflectivity (TRR), suggesting a phonon bottleneck. Using a rate equation model, the emergence of a high-fluence bottleneck is attributed to an abrupt reduction in coupled phonon damping and an increase in exciton dissociation rate. Thus, our work establishes the important role of both excitonic and phononic interactions in the CDW phase transition, as well as the Bose-Einstein condensation of excitons in 1*T*-$TiSe_2$.

Charge density waves (CDWs) are an important component in phase diagrams of many correlated electron systems [1, 2]. Typically observed in low-dimensional materials, the signatures of a CDW phase have been reported in two-dimensional transition metal dichalcogenides (TMDs)[3], cuprate superconductors[4], π-conjugated polymers[5] and metal oxides[6]. The central importance of CDW states arises from the relationship between fluctuations in their order parameter and superconductivity, Mott insulating states, and spin density waves[1, 7]. In the TMD 1*T*-$TiSe_2$ superconductivity appears in proximity to CDW incommensurability[8], which can be achieved by pressure[9], copper doping[10], or electrostatic gating[11]. Thus, understanding of the CDW transition mechanism for this material has attracted considerable scientific interest, especially concerning its driving mechanism[12, 13, 14].

The CDW phase in 1*T*-$TiSe_2$ is achieved upon cooling below T_{CDW} = 202 K, where the hexagonal lattice of the *normal phase* found at room temperature undergoes a reconstruction forming a 2a × 2a × 2c superlattice. This structural fingerprint, denoted here as *periodic lattice distortion* (PLD), occurs together with the opening of an electronic gap (Δ = 130 meV at 80 K), which is large compared to other TMDs exhibiting a CDW[2, 15]. Following early experiments on $TiSe_2$, it was suggested that the CDW state is in fact an excitonic insulator stabilised by Coulomb interactions[16, 17], owing to the semi-metallic character of the band structure, featuring holes in the Se-4p valence band (VB) at the $\bar{\Gamma}$–point and electrons in the Ti-3d conduction band (CB) at the $\bar{M}$-point of the first Brillouin Zone (BZ) (Fig. 1a). Thus, the presence of a PLD and excitons motivated several experimental and theoretical studies aimed at identifying the role of phonons compared to Coulomb interactions[12, 15, 18, 19]. These efforts have highlighted 1*T*-$TiSe_2$ as a model system for studying many-body electron and phonon interactions in condensed matter physics and recently culminated with the report of Bose-Einstein condensation of excitons in this material[20].

When compared to other CDW materials of the TMD family, 1*T*-$TiSe_2$ has small atomic displacements in going from the normal phase structure to the PLD, only ~0.02 Å[21], in stark contrast to changes of up to 0.1 Å observed in 1*T*-TaS_2 for example[18]. The small PLD has been argued to indicate the limited importance of electron-phonon coupling in driving the CDW, thus supporting a purely excitonic mechanism[2, 22]. The typical and consistently reported signatures of the CDW transition in 1*T*-$TiSe_2$ are a downwards shift of the VB energy[23], as a consequence of the CDW gap (Δ) opening, and the presence of backfolded VB appearing in momentum space at $\bar{M}$, consistent with the superlattice structure as sketched in Fig. 1a (the in

plane 2a × 2a reconstruction results in $\bar{M}$ being at the centre of the reconstructed BZ)[24]. However, these important observations, reported by steady-state ARPES, have failed to conclusively identify the excitonic or lattice contribution to the CDW.

Ultrafast spectroscopy is the experimental tool of choice to probe out-of-equilibrium phenomena in correlated electron systems[25, 26, 27, 28]. One of the central themes in this research field is *bottleneck* dynamics, where out-of-equilibrium phonons impede excited carriers from re-joining the CDW or superconducting condensate[25, 28, 29]. Previous ultrafast studies on $TiSe_2$ have not reported such bottleneck effects or used it to disentangle the excitonic and electron-phonon contributions to the CDW[30, 31, 32]. Nevertheless, recent experimental evidence based on optical-pump THz-probe has shown how excitonic order can be transiently suppressed at any sample temperature below T_{CDW}, but with the PLD remaining robust only up to 150 K[13]. Also, signatures of phonon driven oscillations in the CDW recovery have been seen by TR-ARPES clearly suggesting a role for phonons[32]. While such reports cast doubts on a purely excitonic picture, they also open several critical questions: Are phonons and excitons only weakly coupled? How and on what time scale does the lattice dynamics contribute to the CDW recovery? More generally, to what extent is the electron-phonon coupling involved in the CDW formation?

Here, we use TR-ARPES and time resolved optical reflectivity (TRR) to clarify how phonon dynamics in 1*T*-$TiSe_2$ influence the CDW *recovery* following transient perturbation by 30 fs, 1.82 eV light pulses. In TR-ARPES, thanks to a purposely designed combination of time resolution (< 70 fs), energy resolution (~ 53 meV), and sensitivity at low laser fluence (enabled by the 80 kHz laser repetition rate), we are able to probe the VB dynamics in unexplored conditions. We find three distinct *out-of-equilibrium regimes* as a function of excitation fluence. At fluences below F_{th} = 60 μJ cm^{-2} the weakly perturbed CDW recovers within a short timescale of 2 ps. Above this fluence the CDW is still partially present, but its recovery exhibits a bottleneck concomitant with a change in the coherently coupled phonons seen in TRR. With the help of a rate equation model we describe how phonons contribute to the recovery dynamics. Finally, for a fluence above F_{CDW} = 200 μJ cm^{-2}, we enter a third regime with a transient complete suppression of the CDW.

In TR-ARPES, the infrared pump pulse first promotes electrons from the occupied to the unoccupied states with the same momenta, while the subsequent UV probe pulse is used to photoemit electrons and the transient energy dispersion is mapped in momentum space (see

methods section for details). Figures 1b,c,d show the evolution of the TR-ARPES maps at three different time delays between the pump pulse and the probe (6.05 eV) for a $TiSe_2$ single crystal at 80 K. The sample temperature is ideal since it is below T_{CDW} = 202 K, but sufficiently high to allow perturbations to the PLD. Figure 1b shows the TR-ARPES map at -225 fs delay (i.e. before the pump photoexcitation), which reflects the VB dispersion in the vicinity of the $\bar{\Gamma}$ point ($\boldsymbol{k}_{\parallel} = 0$) in the CDW phase along the $\bar{K}$–$\bar{\Gamma}$–$\bar{K}$ direction. The effect of the pump is apparent in Fig. 1c at time delay +25 fs where electrons from the VB have been promoted into a high energy CB for $\boldsymbol{k}$-states at the edges of our detection window. As a high energy CB becomes transiently populated, photoelectron signal is observed above the Fermi level. The effect of the pump and the TR-ARPES maps exhibit features similar to what has been reported in other TR-ARPES studies[31, 33, 34]. Like in other semimetals, [35, 36] carrier relaxation from high energy states occurs within a few hundred fs (see Fig. S10).

The key signature of the CDW is the gap, Δ: Fig 1d shows that the VB is shifted upwards in energy (i.e. Δ is reduced) even at +425 fs delay. This VB shift lasting longer than the pump laser duration (30 fs) is a signature of laser-induced perturbation of Δ. Changes in the VB binding energy are extensively documented in *steady-state* ARPES, when heating the 1*T*-$TiSe_2$ lattice from $T < T_{CDW}$ to the normal phase[15, 23]. In order to accurately study the VB energy shift, we have performed an analysis at the fixed detection angle -14º ($k_{\parallel} \approx$ - 0.1 $Å^{-1}$ for the VB) (dotted white line in Fig.1 b-d) as a function of pump-probe time delay. This angle allows better separation between the Fermi level and the VB, thus avoiding effects due to thermal smearing of the Fermi-Dirac distribution.

As confirmation that the energy shift is indeed a dynamic perturbation of the CDW, and not just heating of the VB electron distribution, we show in Fig. 1e,f the VB dynamics at 80 K and 300 K, respectively. While the data at 80 K exhibit a clear upshift in the VB energy lasting for the whole measurement window of 3 ps, the 300 K trace shows no energy shift and only a loss of intensity due to the transient depletion of electrons in the VB. A closer examination of the VB photo emission spectrum (PES), see Fig. S3, allows us to identify an energy position that shows no dynamics upon pumping at 300 K, i.e. a nodal point in the energy distribution curves that occurs at about 30% of the maximum intensity. This intensity value is used hereafter to monitor the VB dynamics.

The possibility to tune the pump fluence gives additional important insights. Figure 2 illustrates how the VB shift and spectral weight are influenced. A crucial finding of our study is the

measurement of the fluence, F, necessary for a transient closure of Δ, reported to be $\Delta = 0.13$ eV at 80 K[23]. For the analysis, it is important to note that the dominant contribution to the opening of Δ comes from a VB downshift of 0.11 eV at $\bar{\Gamma}$, observed upon cooling from room temperature to 80 K[23]. Figure 2a shows the time dependence of the VB shift for selected pump fluences. The *maximum* VB shift occurs after about 200 fs in all traces, and for 250 μJ cm^{-2} reaches ~0.1 eV. Figure 2b reports the VB shift as a function of fluence at specific time delays corresponding to the maximum shift (dots) and at $t = 3$ ps (triangles), the latter will be discussed below. To gauge the VB maximum shift with respect to the level of CDW perturbation, we have also plotted the shift in the equilibrium VB binding energy as horizontal lines in Fig. 2b, taken from high resolution steady-state ARPES[23] in going from 70 K to 300 K. Two key observations are apparent from the trend of the VB maximum. First, the maximum shift is initially linear for low fluence before reaching a plateau for $F > 93$ μJ cm^{-2} equivalent to a shift in the equilibrium VB binding energy observed at temperatures between 180 K and 200 K. Second, this plateau persists until a critical fluence of $F_{CDW} = 200$ μJ cm^{-2}, beyond which the VB transiently shifts above the 200 K line of equilibrium data and is consistent with complete suppression of Δ and disappearance of CDW order. These nonlinear trends are not due to saturation of absorption from $TiSe_2$ or average laser heating, as shown in Supplementary, but are instead an intrinsic characteristic of the CDW dynamics.

Returning to the VB dynamics in Fig. 2a for the low fluences of 31 and 62 μJ cm^{-2} we find a fast recovery, described by a mono-exponential decay with equal time constants of ~ 770 fs. This leads to a complete VB recovery, i.e. 0 eV shift, at time delays > 2 ps. For higher fluences, multi-exponential decays with lifetimes longer than 1100 fs are found. The inset in Fig. 2a gives a clearer comparison of the same data and plotted on a logarithmic normalised intensity scale. The dynamics can be grouped into two well-defined categories and points to a threshold fluence, F_{th}, between these regimes of fast and slow VB recovery. The residual VB shift at 3 ps (triangles), shown in Fig. 2b, clearly identifies $F_{th} > 62$ μJ cm^{-2}. Note that $F_{th} \cong F_{CDW}/3.3$, and so does not coincide with the complete suppression of Δ occurring at F_{CDW}.

Following these observations, we look at the spectral *intensity* dynamics from the TR-ARPES. The left panel in Fig. 2c shows the spectral weight obtained by integrating the PES up to the Fermi level for $F < F_{th}$, normalised as described in caption. For both fluences the spectral weight is depleted upon photoexcitation and re-established within 500 fs. However, for the 62 μJ cm^{-2} data (orange curve) at a delay > 500 fs the spectral weight shows a small and short-

lived intensity *gain*. Similar behaviour but more pronounced and longer lasting, is observed for the two higher fluences reported in the right panel of Fig. 2c. Photoexcitation with $F \geq F_{th}$, therefore increases spectral weight in the VB. To confirm the origin of this gain we compare the traces at 80 K and 300 K in Fig. 2d. At negative delay, the total intensity measures electrons in the VB up to the Fermi level. This is diminished when going from 300 K to 80 K because CDW formation transfers spectral weight from $\bar{\Gamma}$ to the VB folded at $\bar{M}$ (Fig. 1a). Crucially, the 300 K data in the normal phase do not show any increase in intensity above the initial value. Thus, the observed gain (blue arrow) is caused by the photo-induced unfolding of the VB from $\bar{M}$ to $\bar{\Gamma}$ points and indicates breaking of exciton pairs in the CDW condensate[33], and/or a disturbance of the PLD.

The results of Fig. 2 report the VB dynamics probed in a fluence regime so far unexplored by TR-ARPES in 1*T*-$TiSe_2$. It is important to point out that previous time resolved all-optical experiments in the low fluence regime $F < F_{th}$ have clarified how the initial perturbation of the CDW by fs laser pulses is non-thermal, i.e. it concerns mainly the electronic order in the system represented by the exciton condensate and to a negligible extent the lattice degrees of freedom[13, 14]. This is consistent with electron-electron and electron-exciton scattering times on the order of hundreds of femtoseconds[13]. When discussing possible scenarios for the CDW in $TiSe_2$, we consider that the CDW formation is due to both excitonic *and* lattice interactions, where the relative contributions and relationship are currently unknown. For fluences below F_{th}, the rapid VB recovery is consistent with electronic dynamics and suggests that mainly the excitonic part of the CDW is perturbed. Above F_{th} there is an additional contribution with a longer recovery time, indicating a bottleneck in re-establishing the CDW ground state.

Interestingly, F_{th} identified from the 3 ps data in Fig. 2b corresponds to a VB position at 150 K from steady-state measurements. This is the sample temperature at which recent femtosecond THz experiments reported the disappearance of the phonon fingerprint of the PLD [13]. All together we suggests that the < 200 fs non-thermal shift of ~0.05 eV at F_{th} can be interpreted as the initial excitonic contribution to the CDW. Above F_{th} a second weakening process for Δ sets in, with a maximum contribution of ~0.03 eV, estimated from the 3 ps VB shift at F_{CDW}. A simple picture in which excitonic and phononic contributions can be identified and summed to obtain the full Δ does not apply. Rather we now discuss how phonons can influence the dynamics of Δ.

Understanding of the CDW bottleneck dynamics benefits from monitoring lattice degrees of freedom. While steady-state ARPES experiments can provide indirect information on lattice structure from changes in the electronic band structure, time-resolved experiments allows the dynamics of a subset of phonons to be probed in real time[37]. In TR-ARPES, we observe that below F_{th} the VB dynamics are modulated by periodic oscillations, very likely connected to coherent phonons, whereas above F_{th} their amplitude weakens or is undetectable (Supplementary Information section 4). Oscillations of the VB in TR-ARPES signify the presence of phonons connected with the order parameter, Δ thus it is conceivable that such oscillations will weaken as the CDW is perturbed above F_{th}. Further information on phonon dynamics can be obtained from optical TRR experiments which offer a slightly higher time resolution and probe the change in refractive index of our crystal modulated by phonons. Fig. 3a shows clear oscillations in TRR for all fluences. It is important to note that below $F_{th,}$ both the period and damping time is similar to those seen in TR-ARPES. Figure 3b illustrates examples of the oscillatory component of the signal at different pump fluences after subtraction of an exponential decay. A Fourier transform (FT) of the data in Fig.3b allows us to identify two well separated oscillation frequencies: a low frequency mode at 3.36 THz (112 cm^{-1}) and a high frequency mode at 6.03 THz (201 cm^{-1}). The lower frequency is that of the Raman active A_{1g}* phonon of 1*T*-$TiSe_2$ (Supplementary Figs. S7 and S16). At $F \leq F_{th}$ the A_{1g}* is the most intense coherently coupled phonon with the largest amplitude. This mode is a consequence of the PLD and is not present in the normal phase of 1*T*-$TiSe_2$ [38]. We show in Fig. S7 that the A_{1g}* mode is selectively coupled to the CDW. At $F \geq 132$ $\mu J\ cm^{-2}$ the oscillations are instead dominated by the higher-frequency mode, similar in frequency to the A_{1g} phonon of the normal phase, or two zone-edge modes triggered by a second order process seen in other solids with phase transitions to broken symmetry states[39, 40]. We argue that both assignments for the high frequency 6.03 THz oscillations are consistent with a perturbed PLD and excitation of phonon modes of the normal phase structure (Section 4 in Supplementary information).

The progressive change of amplitude between the selectively coupled phonons (SCP) as the laser intensity increases is symptomatic of two phenomena: (i) A_{1g}* phonons that do not couple coherently to the CDW recovery, (ii) a loss of PLD (disappearance of A_{1g}*) and thus rearrangement of the lattice towards the normal phase, as also supported by the unfolding results (Fig. 2c). Information on phonons is relevant for the bottleneck, since a substantial population of excited vibrational modes (hot phonons) can transfer energy back into the already perturbed exciton condensate and suppress its re-establishment. Most important is the

observation that phonons linked to the normal phase structure modulate the dynamics when the bottleneck in the recovery appears, as shown by the comparison of FT amplitudes and VB shift in Fig. 3d.

We have performed a series of simulations capable of describing the VB dynamics as a function of laser fluence. These are inspired by the Rothwarf-Taylor model which was initially used to describe the equilibration of Cooper pairs in superconductors with hot electrons and phonons[25, 40] and has also been applied to CDW materials[41]. Photoexcitation dynamics in 1*T*-$TiSe_2$ is tracked via three populations: hot carriers (electrons and holes) n_e created by the pump; low energy unbound quasiparticles (QPs) n_q originating from breaking excitons into electrons and holes (a process consistent with Fig. 2c); and a population of the selectively coupled phonons (SCPs), N_p. Following the pump pulse, carriers rapidly relax via electron-electron and electron-phonon scattering, breaking excitons into unbound QPs and exciting the SCPs in the process. Figure 4a outlines the main processes resulting in the relaxation bottleneck. QPs can recombine into the exciton condensate with a rate R by exciting the SCPs further, while absorption of SCPs by the exciton condensate can dissociate excitons to create QPs with a rate η. The SCPs also equilibrate with the bath through anharmonic decay at a rate γ and the ratio η/γ represents the strength of the bottleneck effect. The complete model is discussed in the Supplementary Information.

Figure 4b shows that the VB dynamics can be accurately modelled approximating the VB shift as $\Delta(t) - \Delta_{80K}$ via[25]

$$\Delta(t) = \Delta_{80K}\sqrt{1 - n_q(t)/n_c}\,, \tag{1}$$

where Δ_{80K} = 130 meV is the CDW gap at 80 K(ref.[23]), and n_c is the critical QP density, which we have estimated based on our Hall effect measurements and reports from literature (see Supplementary information). In the model n_e has been determined from the measured laser pulse fluences. The fluence dependence of the two main fitting parameters γ and η, reported in Fig. 4c, shows a correspondence with the VB shift behaviour and to the FT amplitudes of the different coherent phonons in Fig. 3d. The bottleneck effect emerges in the model due to the SCPs becoming simultaneously less damped (smaller γ) and scattering more frequently with excitons (larger η). The substantial change in η with fluence is implicitly accounting within the model for the change in the SCPs energy as the PLD is weakened. A possible correlation between the values of γ^{-1} and the damping time of coherent oscillations τ_{damp} extracted from

TRR experiments appears from Fig. 4c. Future work with structural probes such as TR x-ray diffraction will help to probe the anharmonic decay of SCP in momentum space[39, 41] and thus verify such correlation.

We conclude that below F_{th} only few QPs are excited out of the excitonic condensate and relax by coupling to A_{1g}* phonons characteristic of the PLD. Above F_{th} the excitonic part of the CDW gap is perturbed to an extent where the coupling to the A_{1g}* phonons is weakened and the QP population in excited levels is substantial. Thus, recovery of the CDW experiences a bottleneck controlled by the anharmonic decay of hot phonons. Our results therefore provide evidence that in the out-of-equilibrium phases probed in our experiments, the reformation of the CDW in 1*T*-$TiSe_2$ upon electronic cooling is always influenced by lattice degrees of freedom.

In summary, the CDW dynamics of *1T*-$TiSe_2$ following ultrafast photoexcitation shows different out-of-equilibrium regimes accessed by changing fluence. There exist two distinct regimes below the complete melting of the CDW, one in which the PLD structural order appears robust and a weak perturbation of the excitonic condensate results in a fast recovery time of < 2 ps. For fluences above 60 μJ cm^{-2} the CDW is still present in a metastable state controlled by the lattice degrees of freedom, i.e. hot phonons and partial loss of PLD. Our study conclusively shows that even if Δ can be modelled as the increase of QPs excited out of the exciton condensate (Eq. 1), phonons play a crucial role and can impede the CDW recovery. Future work aiming at controlling the CDW by targeted excitation of phonons with intense THz pulses could represent a new avenue to connect the incommensurate CDW to the superconductivity.[11]

ACKNOWLEDGEMENTS

We thank P. Jones, P. Reddish and W. Lambson for technical support. C.S. and S.K. acknowledges funding and support from the Engineering and Physical Sciences Research Council (EPSRC) Centre for Doctoral Training in Condensed Matter Physics (CDT-CMP), Grant No. EP/L015544/1. S.R.C. and D. W. acknowledge support from EPSRC under grants Nos. EP/P025110/1 and EP/M022188/1, respectively. J.v.W. acknowledges support from a VIDI grant financed by the Netherlands Organization for Scientific Research (NWO). H.H. acknowledges financial support through the Postdoctoral International Fellowship program of

Politecnico Milano. S.F. acknowledges support from EPSRC under grant No. EP/N026691/1. E.D.C. and J.v.W. wish to thank the Royal Society for a Research Grant and an International Exchange Program. E.D.C. acknowledges support from Horizon 2020 (654148, Laserlab-Europe). G.C. acknowledges support by the European Union's Horizon 2020 research and innovation programme under grant agreement No 785219 (GrapheneCore2).

AUTHOR CONTRIBUTIONS

G.C., E.C., and E.D.C designed and managed the research project. H.H. and D.B. performed the TR-ARPES experiments and analysed the data with assistance of C.J.S., G.C., E.C. and C.D.. The crystal growth was performed by C.J.S. Raman experiments were carried out by C.J.S with the assistance of T.B. D.W. performed the calculations of the phonon dispersion. The electrical characterisation was performed by S.K. and S.F.. The modelling was proposed by S.R.C., E.C., J.v.W., C.J.S. and performed by C.J.S.. All authors contributed to the analysis, discussion and interpretation of the results. C.J.S., E.C., and E.D.C. prepared the manuscript with input from all authors.

Corresponding author

Correspondence to Enrico Da Como edc25@bath.ac.uk

Competing interests

The authors declare no competing interests.

Additional information

Supplementary information is available for this paper at

METHODS

Crystal Growth. High quality 1*T*-TiSe2 single crystals were grown using the chemical vapour transport method. Titanium (99.9%) and selenium (>99.9%) powders were sealed inside an evacuated quartz ampoule, together with iodine (>99.9%) which acts as the transport agent. To ensure the correct stoichiometry, a slight selenium excess was included. Single crystals with a typical size of 4 x 4 x 0.1 mm^3 were selected for TR-ARPES measurements. Figure S1 shows resistivity as a function of temperature, where the salient features of the CDW transition appear below 202 K and confirms the high quality of our samples[16].

Experimental setups. TR-ARPES experiments were performed using a custom setup [42] based on a high repetition rate amplified Yb laser (Pharos, Light Conversion) operated at 80 kHz. The pulses from this laser, 290 fs in duration and at 1030 nm, are used to pump a non-collinear optical parametric amplifier (NOPA) which outputs 30 fs pulses at 680 nm (1.82 eV). The NOPA output is used both as pump beam in our TR-ARPES experiment and also to generate the 205 nm (6.05 eV) probe beam for photoemission , through a series of nonlinear optical processes. The time resolution (cross-correlation between pump and probe pulses) is 65 fs, while energy resolution is ~53 meV. In order to measure angle-resolved photoemission we used a time-of-flight detector and spectra for different angles were recorded by rotating the crystal with respect to the analyser (see Supplementary Information for details). Our photon energy allows us to probe up to ± 0.2 $Å^{-1}$ within the BZ, which is sufficient to clearly observe the dynamics of charge carriers in the vicinity of the $\bar{\Gamma}$-point. Before TR-ARPES measurements, the 1*T*-$TiSe_2$ single crystals were cleaved in-situ to expose a clean surface, and oriented using low energy electron diffraction (LEED). Degenerate time-resolved reflectivity (TRR) experiments were performed with the 30 fs pulses at 680 nm as pump and probe beams. They impinged on the sample surface at about 45° with crossed polarisations in order to avoid interference artefacts. All the experiments were performed at a sample temperature ranging from 80 K to 300 K as specified in the text.

Data availability

The data that support the plots within this paper and other findings of this study are available from the corresponding author.

Figures and captions

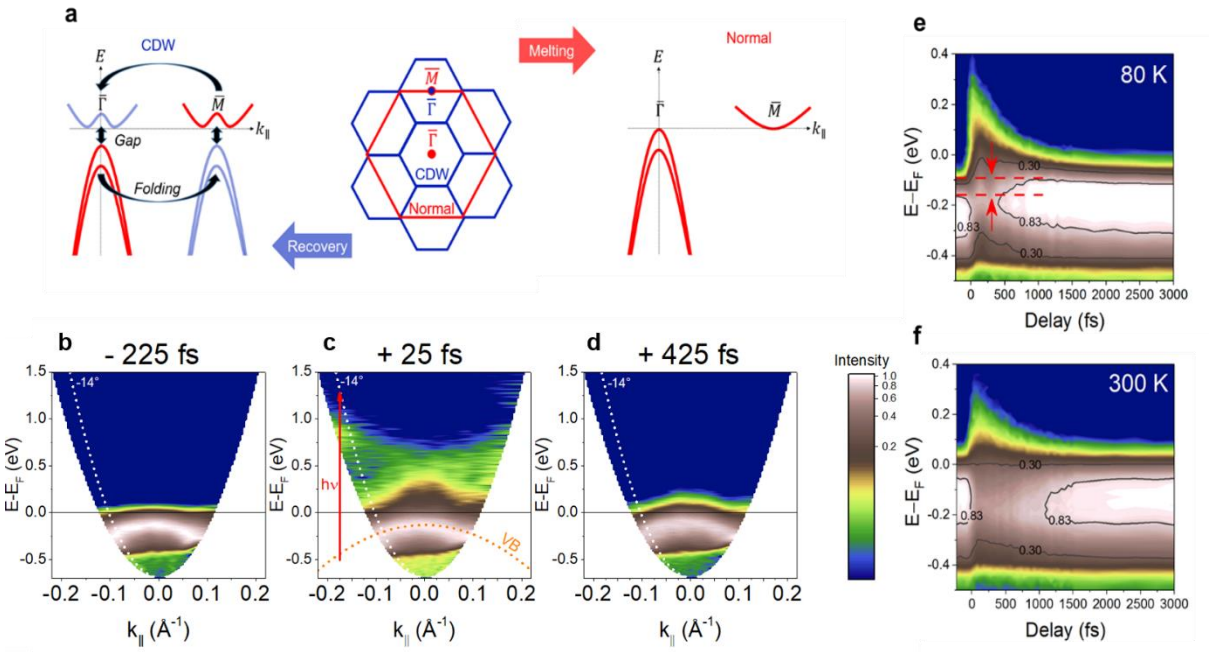

Fig. 1 Valence band dynamics in the CDW and normal phase of 1*T*-TiSe$_2$. a, Sketch of the $TiSe_2$ band structure when switching between the CDW phase (blue) and normal phase (red), together with the projection of the first Brillouin zone (BZ) similar to the one reported in ref. [43]. Band folding arising from the 2a x 2a x 2c PLD is indicated by the curved arrows as $\bar{\Gamma}$ and $\bar{M}$ become equivalent. Vertical arrows show the lowering of the VB maximum due to the formation of a CDW gap, Δ near the Fermi level. **b-d**, Time evolution of the ARPES maps with logarithmic intensity scale (linear scale in Fig. S2) in the CDW phase along the $\bar{K}$–$\bar{\Gamma}$–$\bar{K}$ direction at select pump-probe delays for 125 μJ cm^{-2} fluence. The orange dotted line is a guide to the eye for the VB dispersion. It corresponds to an effective mass of -0.35m_e which is comparable to previous reports[23, 44]. The photon energy of the pump pulse is also shown (red arrows) and the -14° angle for the analysis of the VB dynamics. **e-f,** VB dynamics at 80 K and 300 K, respectively, for a pump fluence of 250 μJ cm^{-2}. The red dashed lines in the 80 K plot indicate the maximum VB shift after pump excitation. The black curves indicate contours at different ARPES intensity. Close inspection of the VB spectra (panel **e-f**) reveal two subbands which are analysed separately in the Supplementary Information for completeness[23].

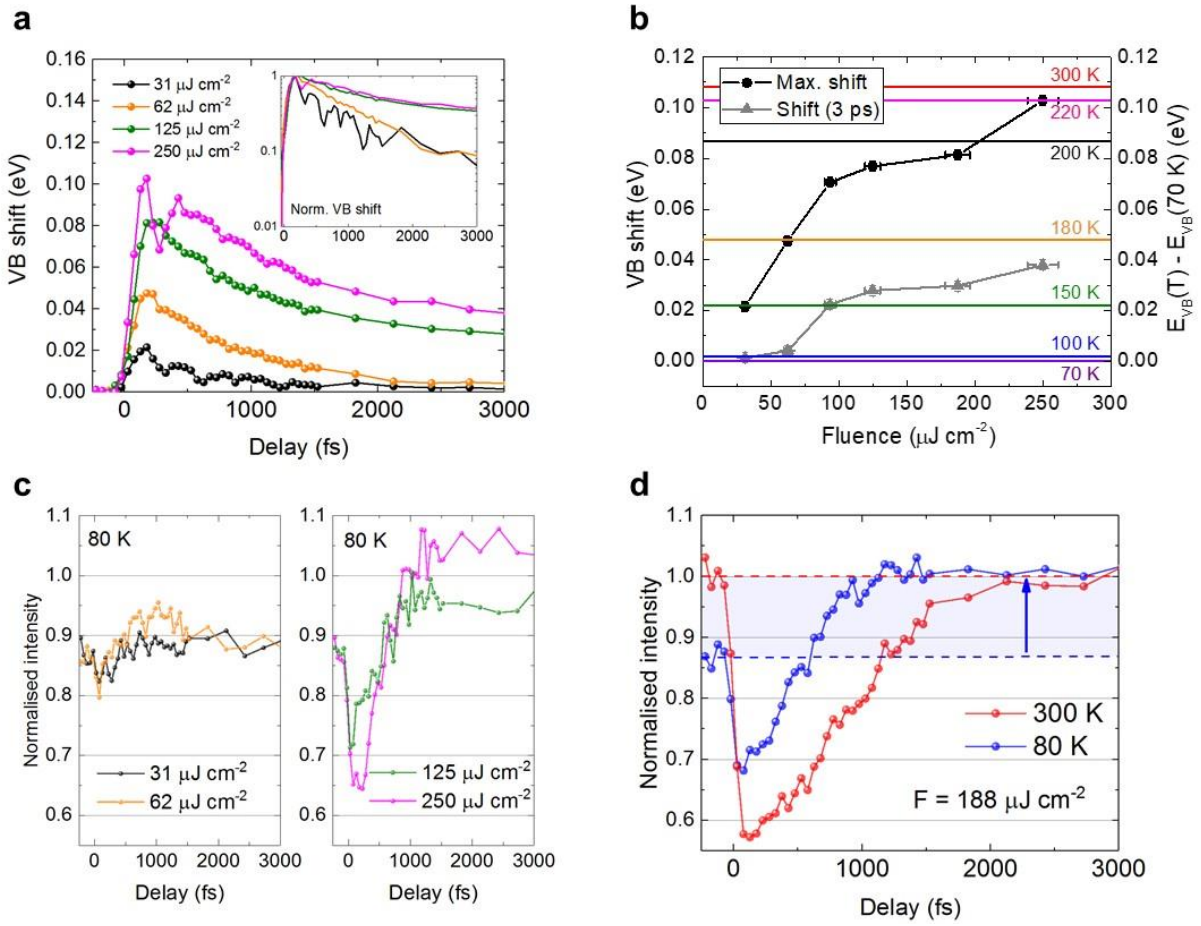

Fig. 2 Fluence dependence of the VB dynamics and spectral intensity. a, VB energy shift, referred to the unperturbed position, as a function of pump-probe time delay at different pump laser fluences as indicated in the main panel,. VB position has been extracted from the contour at 0.3 of the maximum ARPES intensity (example in Fig 1e). The inset shows the same data normalised to the maximum VB energy shift on a logarithmic scale. **b**, Maximum VB shift (dots) and shift at 3 ps (triangles) extracted from panel **a** as a function of fluence. The horizontal lines are linked to the right y-axis and are the shift in VB energy determined by high resolution steady state ARPES as the sample temperature is increased from 70 K, adapted from reference [23]. The VB position at 70 K from steady state ARPES has been set to coincide with the VB energy at negative delays in our experiments. Energy error bars on VB shift data points are < 2 meV. **c**, Intensity of the VB at 80 K and for different laser fluences as indicated, normalised to ARPES intensity at negative delays and at room temperature (shown in **d**). **d**, Comparison between the normalised VB intensity in the CDW phase (80 K) and normal phase (300 K). A gain in intensity is observed in the 80 K data indicated by the blue shaded region.

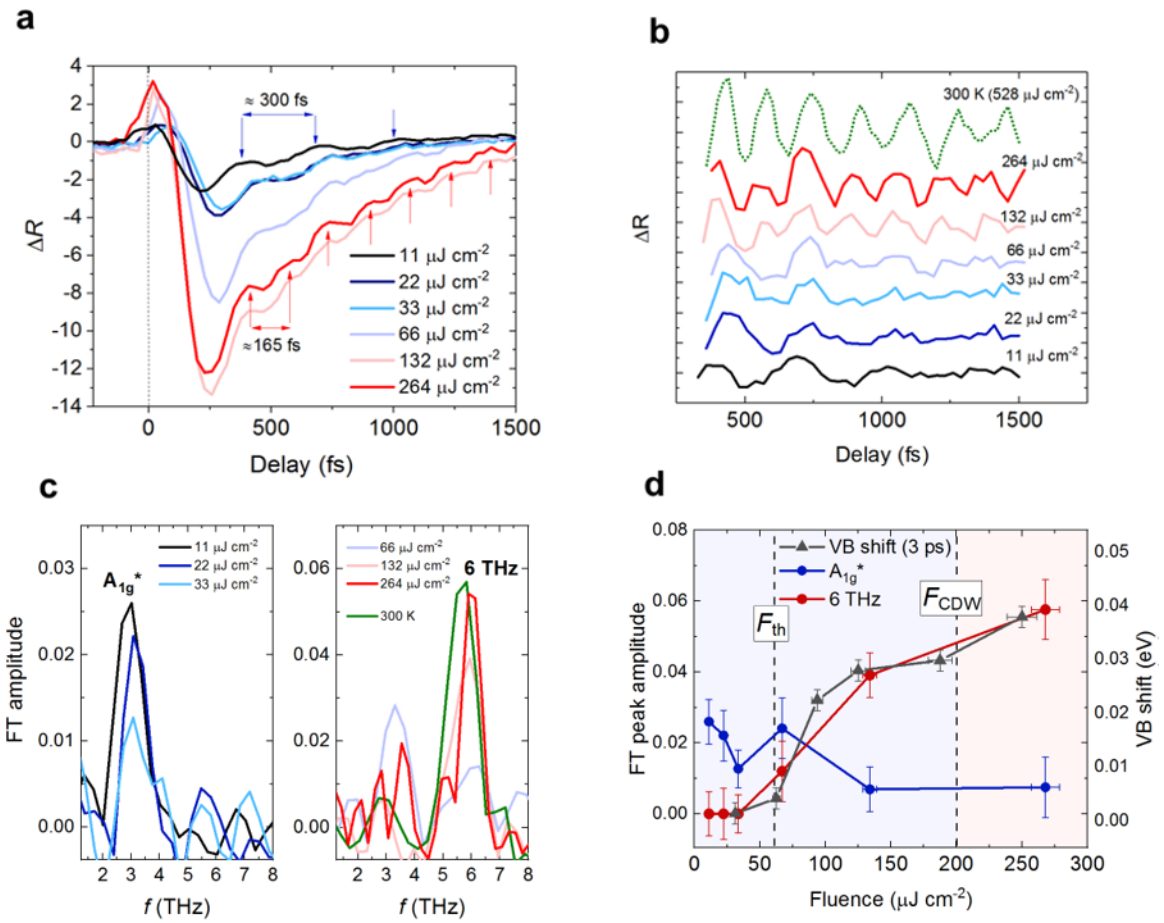

Fig. 3 Coherent coupling to phonons in TRR. a. Coherent phonon oscillations observed by time-resolved reflectivity (TRR) in the CDW phase (80K) at different laser fluences. **b**, Oscillations after subtraction of an exponential decay in the TRR data in panel **a**. **c**, Fourier transform (FT) amplitude for the oscillations in panel b at 80 K together with the normal phase (300 K) for comparison. **d**, FT amplitude of the A_{1g}* and 6 THz modes, as a function of fluence. The VB shift at 3 ps (black triangles) from Fig. 2b is superimposed (right y-axis).

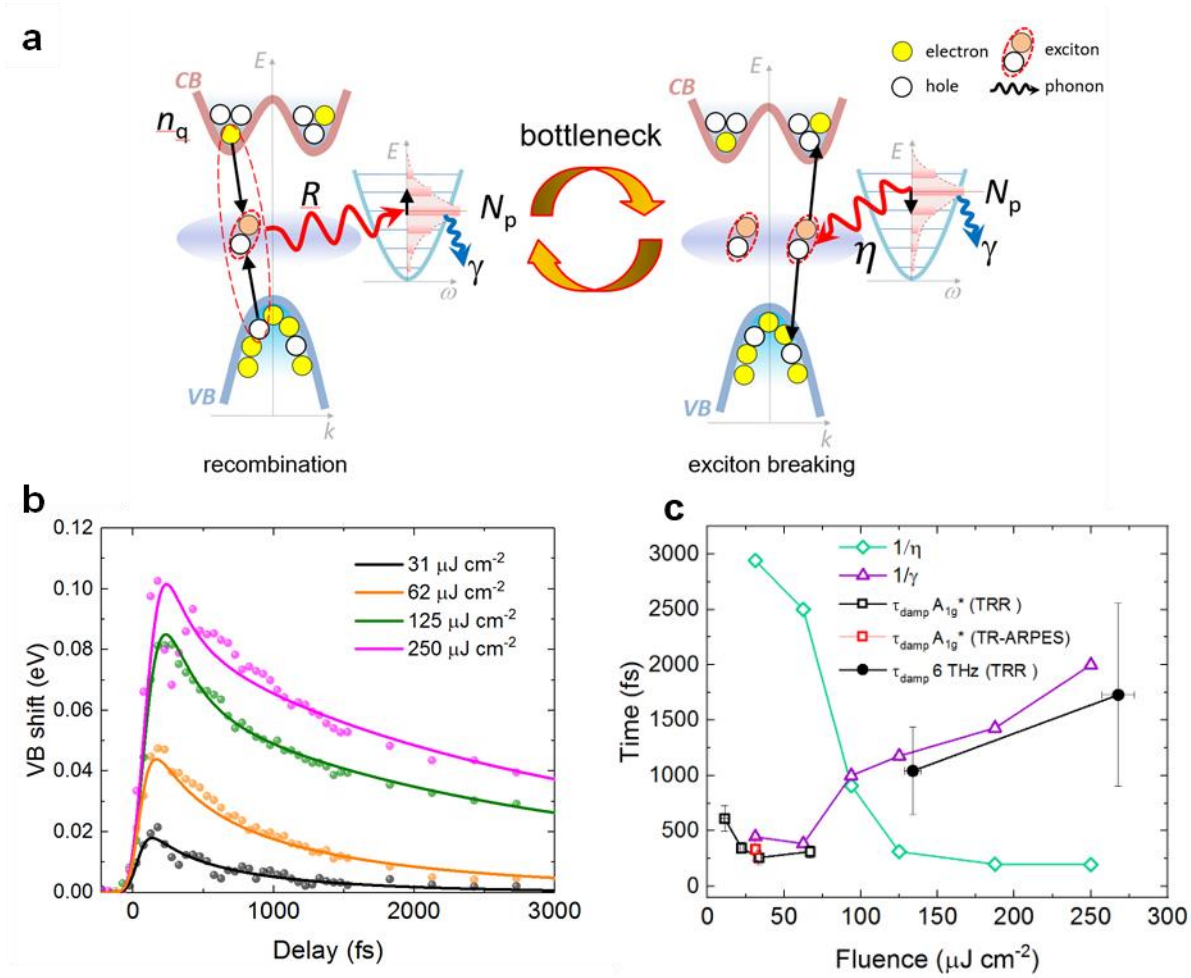

Fig. 4 Modelling of VB dynamics and phonon bottleneck in the CDW recovery. a, Bottleneck involving the quasiparticle population, n_q, and the out of equilibrium SCPs, N_p. The straight black arrows indicate the transition from electron and hole quasiparticles to the exciton condensate in both directions. Red curved arrows indicate the scattering of two quasiparticles with an SCP in the recombination process (left panel) or the scattering of an exciton with an SCP generating two quasiparticles (right). γ is used to indicate the anharmonic phonon-phonon scattering with the thermal bath. The orange arrows illustrate the iterative dynamics between recombination and re-excitation influenced by γ. The Supplementary information (Fig. S13) includes a further diagram illustrating the fast photoexcitation process preceding this bottleneck dynamics. **b**, VB dynamics extracted from the model (solid curves) overlaid with the TR-ARPES data (dots) from Fig. 2a. **c**, Fluence dependence of the fitting parameters $1/\eta$ (green diamonds) and $1/\gamma$ (purple triangles) together with damping times, τ_{damp}, from experiments as indicated in the legend. The τ_{damp} of different phonon modes are shown separately.

References

1. Chen CW, Choe J, Morosan E. Charge density waves in strongly correlated electron systems. *Rep Prog Phys* 2016, **79**(8)**:** 084505.

2. Rossnagel K. On the origin of charge-density waves in select layered transition-metal dichalcogenides. *J Phys-Condes Matter* 2011, **23**(21)**:** 213001.

3. Wilson JA, Di Salvo FJ, Mahajan S. Charge-Density Waves and superlattices in metallic layered transition-metal dichlacogenides. *Adv Phys* 1975, **24**(2)**:** 117-201.

4. Gerber S, Jang H, Nojiri H, Matsuzawa S, Yasumura H, Bonn DA*, et al.* Three-dimensional charge density wave order in YBa2Cu3O6.67 at high magnetic fields. *Science* 2015, **350**(6263)**:** 949-952.

5. Osterbacka R, Jiang XM, An CP, Horovitz B, Vardeny ZV. Photoinduced quantum interference antiresonances in pi-conjugated polymers. *Phys Rev Lett* 2002, **88**(22)**:** 4.

6. Sato M, Fujishita H, Sato S, Hoshino S. Neutron inelastic scatterning and X-ray structural study of the charge density wave state in K0.3MOO3. *Journal of Physics C-Solid State Physics* 1985, **18**(13)**:** 2603-2614.

7. Monceau P. Electronic crystals: an experimental overview. *Adv Phys* 2012, **61**(4)**:** 325-581.

8. Joe YI, Chen XM, Ghaemi P, Finkelstein KD, de la Pena GA, Gan Y*, et al.* Emergence of charge density wave domain walls above the superconducting dome in 1T-TiSe2. *Nature Phys* 2014, **10**(6)**:** 421-425.

9. Kusmartseva AF, Sipos B, Berger H, Forro L, Tutis E. Pressure Induced Superconductivity in Pristine 1T-TiSe2. *Phys Rev Lett* 2009, **103**(23)**:** 236401.

10. Morosan E, Zandbergen HW, Dennis BS, Bos JWG, Onose Y, Klimczuk T*, et al.* Superconductivity in CuxTiSe2. *Nature Phys* 2006, **2**(8)**:** 544-550.

11. Li LJ, O'Farrell ECT, Loh KP, Eda G, Ozyilmaz B, Neto AHC. Controlling many-body states by the electric-field effect in a two-dimensional material. *Nature* 2016, **529**(7585)**:** 185-189.

12. van Wezel J, Nahai-Williamson P, Saxena SS. Exciton-phonon-driven charge density wave in TiSe2. *Phys Rev B* 2010, **81**(16)**:** 165109.

13. Porer M, Leierseder U, Menard JM, Dachraoui H, Mouchliadis L, Perakis IE*, et al.* Non-thermal separation of electronic and structural orders in a persisting charge density wave. *Nature Mater* 2014, **13**(9)**:** 857-861.

14. Mohr-Vorobeva E, Johnson SL, Beaud P, Staub U, De Souza R, Milne C*, et al.* Nonthermal Melting of a Charge Density Wave in TiSe2. *Phys Rev Lett* 2011, **107**(3)**:** 036403.

15. Rossnagel K, Kipp L, Skibowski M. Charge-density-wave phase transition in 1T-TiSe2: Excitonic insulator versus band-type Jahn-Teller mechanism. *Phys Rev B* 2002, **65**(23)**:** 235101.

16. Di Salvo FJ, Moncton DE, Waszczak JV. Electronic properties and superlattice formation in semimetal TiSe2. *Phys Rev B* 1976, **14**(10)**:** 4321-4328.

17. Jerome D, Rice TM, Kohn W. Excitonic insulator. *Physical Review* 1967, **158**(2)**:** 462-475.

18. Cercellier H, Monney C, Clerc F, Battaglia C, Despont L, Garnier MG*, et al.* Evidence for an excitonic insulator phase in 1T-TiSe2. *Phys Rev Lett* 2007, **99**(14)**:** 146403.

19. Li G, Hu WZ, Qian D, Hsieh D, Hasan MZ, Morosan E*, et al.* Semimetal-to-semimetal charge density wave transition in 1T-TiSe2. *Phys Rev Lett* 2007, **99**(2)**:** 027404.

20. Kogar A, Rak MS, Vig S, Husain AA, Flicker F, Il Joe Y*, et al.* Signatures of exciton condensation in a transition metal dichalcogenide. *Science* 2017, **358**(6368)**:** 1314-1317.

21. Bianco R, Calandra M, Mauri F. Electronic and vibrational properties of TiSe2 in the charge-density-wave phase from first principles. *Phys Rev B* 2015, **92**(9)**:** 094107.

22. Yoshida Y, Motizuki K. Electron lattice interaction and lattice instability of 1T-TiSe2. *J Phys Soc Jpn* 1980, **49**(3)**:** 898-905.

23. Chen P, Chan YH, Fang XY, Mo SK, Hussain Z, Fedorov AV*, et al.* Hidden Order and Dimensional Crossover of the Charge Density Waves in TiSe2. *Scientific Reports* 2016, **6:** 37910.

24. Pillo T, Hayoz J, Berger H, Levy F, Schlapbach L, Aebi P. Photoemission of bands above the Fermi level: The excitonic insulator phase transition in 1T-TiSe2. *Phys Rev B* 2000, **61**(23)**:** 16213-16222.

25. Giannetti C, Capone M, Fausti D, Fabrizio M, Parmigiani F, Mihailovic D. Ultrafast optical spectroscopy of strongly correlated materials and high-temperature superconductors: a non-equilibrium approach. *Adv Phys* 2016, **65**(2)**:** 58-238.

26. Vogelgesang S, Storeck G, Horstmann JG, Diekmann T, Sivis M, Schramm S*, et al.* Phase ordering of charge density waves traced by ultrafast low-energy electron diffraction. *Nature Phys* 2018, **14**(2)**:** 184-190.

27. Boschini F, da Silva Neto EH, Razzoli E, Zonno M, Peli S, Day RP*, et al.* Collapse of superconductivity in cuprates via ultrafast quenching of phase coherence. *Nature Mater* 2018, **17**(5)**:** 416-420.

28. Orenstein J. Ultrafast spectroscopy of Quantum Materials. *Phys Today* 2012, **65**(9)**:** 44-50.

29. Han SG, Vardeny ZV, Wong KS, Symko OG, Koren G. Femtosecond optical-detection of quasiparticle dynamics in high-TC YBA2CU3O7 superconducting thin films. *Phys Rev Lett* 1990, **65**(21)**:** 2708-2711.

30. Hellmann S, Rohwer T, Kallane M, Hanff K, Sohrt C, Stange A*, et al.* Time-domain classification of charge-density-wave insulators. *Nature Comm* 2012, **3:** 1069.

31. Rohwer T, Hellmann S, Wiesenmayer M, Sohrt C, Stange A, Slomski B*, et al.* Collapse of long-range charge order tracked by time-resolved photoemission at high momenta. *Nature* 2011, **471**(7339)**:** 490-493.

32. Monney C, Puppin M, Nicholson CW, Hoesch M, Chapman RT, Springate E*, et al.* Revealing the role of electrons and phonons in the ultrafast recovery of charge density wave correlations in 1T-TiSe2. *Phys Rev B* 2016, **94**(16)**:** 165165.

33. Mathias S, Eich S, Urbancic J, Michael S, Carr AV, Emmerich S*, et al.* Self-amplified photo-induced gap quenching in a correlated electron material. *Nature Comm* 2016, **7:** 12902.

34. Rohde G, Rohwer T, Sohrt C, Stange A, Hellmann S, Yang LX*, et al.* Tracking the relaxation pathway of photo-excited electrons in 1T-TiSe2. *Eur Phys J-Spec Top* 2013, **222**(5)**:** 997-1004.

35. Limmer T, Feldmann J, Da Como E. Carrier Lifetime in Exfoliated Few-Layer Graphene Determined from Intersubband Optical Transitions. *Phys Rev Lett* 2013, **110**(21)**:** 217406.

36. Bugini D, Boschini F, Hedayat H, Yi H, Chen C, Zhou X*, et al.* Ultrafast spin-polarized electron dynamics in the unoccupied topological surface state of Bi 2 Se 3. *Journal of Physics: Condensed Matter* 2017, **29**(30)**:** 30LT01.

37. Perfetti L, Loukakos PA, Lisowski M, Bovensiepen U, Berger H, Biermann S*, et al.* Time evolution of the electronic structure of 1T-TaS2 through the insulator-metal transition. *Phys Rev Lett* 2006, **97**(6)**:** 067402.

38. Holy JA, Woo KC, Klein MV, Brown FC. Raman and infrared studies of superlattice formation in TiSe2. *Phys Rev B* 1977, **16**(8)**:** 3628-3637.

39. Huber T, Mariager SO, Ferrer A, Schäfer H, Johnson JA, Grübel S*, et al.* Coherent Structural Dynamics of a Prototypical Charge-Density-Wave-to-Metal Transition. *Phys Rev Lett* 2014, **113**(2)**:** 026401.

40. Rettig L, Cortés R, Chu JH, Fisher IR, Schmitt F, Moore RG*, et al.* Persistent order due to transiently enhanced nesting in an electronically excited charge density wave. *Nature Comm* 2016, **7:** 10459.

41. Beaud P, Caviezel A, Mariager SO, Rettig L, Ingold G, Dornes C*, et al.* A time-dependent order parameter for ultrafast photoinduced phase transitions. *Nature Mater* 2014, **13**(10)**:** 923-927.

42. Boschini F, Hedayat H, Dallera C, Farinello P, Manzoni C, Magrez A*, et al.* An innovative Yb-based ultrafast deep ultraviolet source for time-resolved photoemission experiments. *Rev Scien Instrum* 2014, **85**(12)**:** 123903.

43. Monney C, Schwier EF, Garnier MG, Mariotti N, Didiot C, Cercellier H*, et al.* Probing the exciton condensate phase in 1T-TiSe2 with photoemission. *New J Phys* 2010, **12:** 32.

44. Kidd TE, Miller T, Chou MY, Chiang TC. Electron-Hole Coupling and the Charge Density Wave Transition in ${\mathrm{TiSe}}_{2}$. *Phys Rev Lett* 2002, **88**(22)**:** 226402.